

1 **Proxy reconstruction of ultraviolet-B irradiance at the Earth's surface, and**  
2 **its relationship with solar activity and ozone thickness**

3  
4 **P. E. Jardine<sup>1,2</sup>, W. T. Fraser<sup>3,2</sup>, W. D. Gosling<sup>4,2</sup>, C. N. Roberts<sup>5</sup>, W. J. Eastwood<sup>6</sup> and B.**  
5 **H. Lomax<sup>7</sup>**

6 <sup>1</sup>Institute of Geology and Palaeontology, University of Münster, 48149 Münster, Germany.

7 <sup>2</sup>School of Environment, Earth and Ecosystem Sciences, The Open University, Walton Hall,  
8 Milton Keynes, MK7 6AA, UK.

9 <sup>3</sup>Geography, Department of Social Sciences, Oxford Brookes University, Oxford OX3 0BP,  
10 UK.

11 <sup>4</sup>Department of Ecosystem and Landscape Dynamics, Institute of Biodiversity & Ecosystem  
12 Dynamics (IBED), University of Amsterdam, 1090 GE Amsterdam, The Netherlands.

13 <sup>5</sup>School of Geography, Earth and Environmental Sciences, University of Plymouth, PL4 8AA,  
14 UK.

15 <sup>6</sup>School of Geography, Earth and Environmental Sciences, University of Birmingham, B15  
16 2TT, UK.

17 <sup>7</sup>Agriculture and Environmental Science, University of Nottingham, Sutton Bonington  
18 Campus, Leicestershire, LE12 5RD, UK.

19  
20 **Corresponding author:**

21 Phillip Jardine, Institute of Geology and Palaeontology, University of Münster, 48149  
22 Münster, Germany.

23 Email: Phillip Jardine ([jardine@uni-muenster.de](mailto:jardine@uni-muenster.de)).

## 26 **Abstract**

27 Solar ultraviolet-B (UV-B) irradiance that reaches the Earth's surface acts as a biotic stressor  
28 and has the potential to modify ecological and environmental functioning. The challenges of  
29 reconstructing UV irradiance prior to the satellite era mean that there is uncertainty over long-  
30 term surface UV-B patterns, especially in relation to variations in solar activity over  
31 centennial and millennial timescales. Here, we reconstruct surface UV-B irradiance over the  
32 last 650 years using a novel UV-B proxy based on the chemical signature of pollen grains.  
33 We demonstrate a statistically significant positive relationship between the abundance of UV-  
34 B absorbing compounds in *Pinus* pollen and modelled solar UV-B irradiance. These results  
35 show that trends in surface UV-B follow the overall solar activity pattern over centennial  
36 timescales, and that variations in solar output are the dominant control on surface level UV-B  
37 flux, rather than solar modulated changes in ozone thickness. The *Pinus* biochemical response  
38 demonstrated here confirms the potential for solar activity driven surface UV-B variations to  
39 impact upon terrestrial biotas and environments over long timescales.

40

41 **Keywords:** Ultraviolet-B irradiance; pollen; vegetation; palaeoclimate; solar activity; ozone

42

## 43 **Introduction**

44 The role of solar activity in influencing the Earth system has received an increase in  
45 attention over recent years (Ermolli et al., 2013; Gray et al., 2010; Solanki et al., 2013).  
46 Predominantly, the focus has been on total solar irradiance (TSI, defined as the amount of  
47 solar energy reaching the upper atmosphere) and its contributions to climatic changes versus  
48 anthropogenic inputs (Solanki et al., 2013). In addition to TSI, which affects temperature and  
49 atmospheric circulation patterns through 'bottom up' warming of the Earth's surface, there is  
50 a growing awareness of the importance of ultraviolet (UV) irradiance as a climate forcing  
51 mechanism (Gray et al., 2010; Ineson et al., 2015). UV irradiance stimulates production and

52 destruction of ozone via absorption driven processes (the Chapman cycle), resulting in a  
53 warming of the stratosphere and exerting a ‘top down’ influence on regional climatic and  
54 oceanic patterns through dynamical coupling with the underlying troposphere (Ermolli et al.,  
55 2013; Gray et al., 2010; Ineson et al., 2015; Solanki et al., 2013).

56

57         Solar UV-B (280-315 nm) radiation that reaches the Earth’s surface (referred to  
58 hereafter as surface UV-B) is an important stressor on biotic systems, and has the potential to  
59 drive larger-scale ecosystem-level processes (Rozema et al., 1997). As well as directly  
60 damaging DNA, enhanced UV-B levels can lead to morphological and phenological changes  
61 in plants and possibly alter competitive relationships among species (Caldwell et al., 1998;  
62 Rozema et al., 1997). UV-B stimulates production of secondary metabolites that in part act as  
63 UV protective compounds, which are both a metabolic cost to the plant and can influence  
64 herbivory levels, plant decomposition and carbon cycling (Meijkamp et al., 1999; Rozema et  
65 al., 1997). Increased surface UV-B can also directly enhance leaf litter decomposition through  
66 photodegradation, and impact upon the activities of organisms such as animals, fungi and  
67 bacteria that play a role in decomposition and nutrient cycling (Gehrke et al., 1995; Rozema  
68 et al., 1997). While much attention has been focused on multidecadal increases in surface  
69 UV-B flux due to anthropogenic reductions in ozone thickness (Caldwell et al., 1998; Lomax  
70 et al., 2008), considerably less is known about the surface UV-B changes that result from long  
71 term (centuries to millennia) variations in solar activity, and what impact these have on  
72 ecological and environmental functioning.

73

74         Temporal changes in surface UV-B flux are a result of variations in solar UV  
75 irradiance, ozone thickness, and their interaction. Variations in solar activity have been  
76 characterized by satellite measurements since 1978 (all dates given in calendar years CE), and  
77 historical proxies such as sunspot counts from 1610 and cosmogenic radionuclides (primarily

78  $^{10}\text{Be}$  and  $^{14}\text{C}$ ) through the Holocene (Solanki et al., 2013; Steinhilber et al., 2012; Svalgaard  
79 and Schatten, 2016). These indicators reveal solar cycles ranging in length from  $\sim 27$  days to  
80 several millennia, as well as irregularly spaced, sustained ‘Grand’ minima and maxima of  
81 solar activity (e.g. the Maunder Minimum,  $\sim 1645$  to 1710) (Solanki et al., 2013; Usoskin,  
82 2017). Temporal variations in solar UV irradiance are still poorly understood, partly because  
83 of the discontinuous nature of spectral solar irradiance (SSI) satellite measurements  
84 (Haberreiter et al., 2017), but mostly because of the challenges of reconstructing UV  
85 irradiance beyond the satellite era. Nevertheless, SSI satellite measurements have revealed  
86 UV cycles (in particular the 11-year solar cycle) in phase with those of TSI (Usoskin, 2017),  
87 and the long term constancy of this relationship has been assumed in models of TSI and SSI  
88 such as the semi-empirical SATIRE-T model (Spectral And Total Irradiance REconstructions  
89 for the Telescope era), which has provided UV reconstructions back to the Maunder  
90 Minimum (Krivova et al., 2010), and the empirical NRLSSI2 model (Naval Research  
91 Laboratory Solar Spectral Irradiance), which has recently been extended back to 850 (Lean,  
92 2018).

93  
94         Increased UV-C (100-280 nm) flux during enhanced solar activity stimulates ozone  
95 production, limiting the flow of UV-B to the Earth surface. It follows that while incoming  
96 (top of atmosphere) UV-B and TSI may be correlated through time, surface level UV-B will  
97 be anticorrelated with both (Rampelotto et al., 2009; Rozema et al., 2002), and this is  
98 supported by ground based measurements of UV-B across the 11 year solar cycle  
99 (Rampelotto et al., 2009). Rozema et al. (2002) hypothesized that this relationship will be  
100 consistent across longer-term solar variations, with higher levels of surface UV-B flux during  
101 solar activity lows such as the Maunder Minimum, even though overall UV and TSI are  
102 reduced. Empirical evidence to test this hypothesis is currently lacking, however. Surface  
103 UV-B proxy reconstructions based on the abundance of photoprotective pigments in fossil

104 cladocera (water flea) carapaces in arctic and subarctic lakes (Nevalainen et al., 2015, 2016,  
105 2018) demonstrated a positive correlation between surface UV-B and solar activity over the  
106 last millennium, which is the opposite pattern to that predicted by Rozema et al. (2002).  
107 However, UV-B proxies based on aquatic organisms such as cladocerans are influenced by  
108 water transparency as well as ambient UV-B, and so relate at least in part to local climatic and  
109 vegetation conditions and anthropogenic land use changes (Nevalainen et al., 2015, 2018).  
110 Although these impacts should have been limited in the arctic lake records used by  
111 Nevalainen et al. (2016), where water and UV transparency are high, it is still not clear what  
112 the long-term relationship between solar activity and surface UV-B is, and therefore what  
113 biotic and environmental impacts can be expected from solar variability in the future.

114

115         To address these uncertainties, we take advantage of a novel proxy for surface UV-B  
116 irradiance based on the chemistry of pollen grains (Fraser et al., 2014; Rozema et al., 2001;  
117 Seddon et al., 2019). Plants produce UV absorbing compounds (UACs) to protect their cells  
118 from the harmful effects of UV-B, and up-regulate production in response to increased UV-B  
119 doses (Fraser et al., 2014; Gao et al., 2004; Lomax et al., 2008; Rozema et al., 2001; Singh et  
120 al., 2014). Pollen grains and spores preserve well in the fossil record because their outer wall,  
121 or exine, is made of sporopollenin, a highly resistant biopolymer (Mackenzie et al., 2015).  
122 Critically, the UAC signal within the exine is also preserved (Jardine et al., 2016), and  
123 remains stable over geological time (Fraser et al., 2012). Therefore, by measuring the  
124 concentration of UACs in fossil and sub-fossil pollen grains, UV-B flux in the past can be  
125 reconstructed (Blokker et al., 2005, 2006; Fraser et al., 2014; Jardine et al., 2016; Lomax et  
126 al., 2008; Rozema et al. 2001; Seddon et al., 2019; Willis et al., 2011).

127

128         The UV-B response mechanism is thought to be an ancient evolutionary adaptation to  
129 terrestrial environments and occurs across the land plant phylogeny (Christie et al., 2012;

130 Jardine et al., 2016; Rizzini et al., 2011; Rozema et al., 1997), which means that a wide array  
131 of taxa are available for sampling from the pollen and spore record. To date, a positive  
132 correlation between UV-B and sporopollenin UAC levels has been demonstrated for  
133 *Lycopodium* (clubmoss) (Fraser et al., 2011; Jardine et al., 2016, 2017; Lomax et al., 2008,  
134 2012; Watson et al., 2007), *Pinus* (pine) (Willis et al., 2011), *Cedrus atlantica* (Atlas cedar)  
135 (Bell et al., 2018), *Vicia faba* (broad or fava bean) (Rozema et al., 2001), and Poaceae  
136 (grasses) (Jardine et al., 2016), confirming the broad phylogenetic applicability of the UAC  
137 proxy. Furthermore, because this proxy is based on terrestrial plants, it is less biased by  
138 changes in the surrounding environment than those derived from aquatic organisms. UAC  
139 concentrations in pollen and spores are determined by the UV dose experienced by the parent  
140 plant, and are thought to represent the clear skies maximum UV level across the growing or  
141 pollen/spore production period (i.e. a timescale of several weeks prior to pollen/spore release)  
142 (Jardine et al., 2016; Lomax et al., 2012). The impact of short-term variations in cloudiness  
143 on UAC levels should therefore be limited, and inter-annual comparisons of UV-B flux can  
144 be achieved. Since the UAC proxy detects surface UV-B flux it is sensitive to changes in  
145 ozone column thickness (Lomax et al., 2008), which means that variations in surface-level  
146 UV-B caused by changes in ozone through time can be recovered.

147

148 Here, we use a maar lake sedimentary record from Nar Gölü in central Turkey, and  
149 analyse UAC concentrations in *Pinus* pollen to reconstruct surface UV-B flux over the last  
150 650 years. This record is then used to test for the correlation between surface UV-B and  
151 modelled solar UV-B irradiance, following the assumption that TSI and solar UV-B  
152 irradiance will vary in phase through time. A negative correlation would support the  
153 hypothesis of Rozema et al. (2002), with solar activity highs leading to ozone production and  
154 decreased UV-B flux to the surface. A positive correlation would support the cladoceran UV-  
155 B reconstructions of Nevalainen et al., (2015, 2016, 2018), and would suggest that the

156 relationship between solar activity and ozone thickness observed on shorter timescales (e.g.  
157 Rampelotto et al., 2009) cannot simply be scaled up across centuries and millennia.

158

## 159 **Materials and Methods**

160 Nar Gölü (38°20'24"N, 34°27'23"E; 1363 m a.s.l.) is a maar lake in central Turkey,  
161 ~0.7 km<sup>2</sup> in area and ~26 m deep, with a sediment record extending through the Holocene and  
162 into the last glacial (Dean et al., 2015). The upper 2500 years of the sedimentary sequence is  
163 continuously annually laminated (varved), which has allowed for a precise chronology to be  
164 developed (Dean et al., 2015; Jones et al., 2005). The Nar Gölü sediment record has been the  
165 focus of previous sedimentological, mineralogical, palynological and geochemical research  
166 (Dean et al., 2013, 2015; England et al., 2008; Jones et al., 2005, 2006).

167

168 The sediment core used in this study was collected in 2001, and the pollen samples  
169 were initially documented in England et al. (2008). The age model for this core was based on  
170 varve counting, which was carried out independently by two workers, who recounted until  
171 agreement to within 3 laminae for each 6 cm section of core was reached (Jones et al., 2005).  
172 Replication of varve counts from additional cores has provided a maximum age uncertainty of  
173 2.5% of the given age (Jones et al., 2006). The pollen samples were collected at ~20 year  
174 inter-sample resolution, with most samples representing 3 (sometimes 4 or 5) years of  
175 sediment accumulation. The whole sequence covers 640 years and ~160 cm of sediment core.  
176 The samples were processed according to standard palynological protocols, using 10% HCl,  
177 10% NaOH, 60% HF, and acetolysis (England et al., 2008). We used the same pollen  
178 preparations in this study to maintain stratigraphic consistency with the pollen count data, and  
179 because standard processing protocols, including acetolysis (oxidation), do not impact upon  
180 the recoverability of variations in UAC concentrations across samples (Jardine et al., 2015,

181 2016, 2017). Furthermore, Bell (2018) showed that UAC levels were similar in acetolysed  
182 and untreated *Pinus* pollen.

183

184 We selected *Pinus* as the target taxon because it is abundant through most of the upper  
185 part of the Nar Gölü record, with relative abundances of 13% to 45% of the pollen sum and  
186 influx rates of 300 to 4400 cm<sup>2</sup>/year (England et al., 2008). Furthermore, compared to lower  
187 stature vegetation the impact of localized shading on UV reconstructions (Fraser et al., 2011;  
188 Jardine et al., 2016) should be minimal. A positive association between UAC levels and UV-  
189 B has also previously been demonstrated for *Pinus* pollen, across both a modern latitudinal  
190 gradient and over the last 9.5 kyr (Willis et al., 2011), suggesting that a measurable signal is  
191 recoverable from the Nar Gölü *Pinus* pollen record. *Pinus* pollen within the Nar Gölü  
192 sediments represents mostly regional rather than local vegetation, and is mostly derived from  
193 the Taurus Mountains >70 km south and southeast of Nar Gölü, although *Pinus* was also  
194 planted near the lake in the 1980s (England et al., 2008). In the modern day, the three main  
195 *Pinus* species in this region are *Pinus brutia*, *Pinus nigra* and *Pinus sylvestris* (Woldring and  
196 Bottema, 2003), and these are anticipated to have been the major contributors to the Nar Gölü  
197 *Pinus* pollen record during the study interval.

198

199 We used Fourier Transform Infrared (FTIR) microspectroscopy to generate the  
200 chemical data, because previous analyses (Bell et al., 2018; Fraser et al., 2011; Jardine et al.,  
201 2016, 2017; Lomax et al., 2008, 2012; Watson et al., 2007) have shown that this can  
202 successfully capture variations in UAC abundances at small sample sizes. To prepare the  
203 samples for FTIR analysis, individual *Pinus* pollen grains were picked out from the processed  
204 sediment samples and mounted on ZnSe windows. To pick the pollen grains we used an  
205 inverted microscope with a micromanipulator attachment, the full set-up comprising  
206 Narishige MMN-1 and MMO-202ND course and fine control micromanipulators, an IM-11-2



207 pneumatic microinjector, with a Microtec IM-2 inverted microscope. The picked pollen grains  
208 were arranged in groups of 4 to 5 grains on the ZnSe windows, with 5 replicate groups per  
209 sample. This means that each FTIR spectrum represents 4 or 5 pollen grains, and each pollen  
210 sample is represented by 5 replicate FTIR spectra. We generated the data using a Thermo  
211 Scientific (Waltham, MA, USA) Nicolet Nexus FTIR bench unit connected to a Continuum  
212 IR microscope fitted with an MCT-A liquid nitrogen-cooled detector and a ReFlachromat 15x  
213 objective lens. FTIR spectra were generated in transmission mode using a microscope  
214 aperture of 100 x 100  $\mu\text{m}$  recording the mean of 256 scans with a resolution of  $1.928\text{ cm}^{-1}$   
215 wavenumbers. Five of the 33 samples in the study interval had insufficient *Pinus* pollen for  
216 FTIR analysis, resulting in a dataset of 28 samples.

217  
218 Peak height measurement and data analysis were carried out in R v3.4.0 (R Core  
219 Team, 2017). The package ‘baseline’ v1.2-1 (Liland and Mevik, 2015) was used to baseline  
220 correct the IR spectra, by subtracting a 2nd order polynomial baseline from each spectrum  
221 (Figure 1). We quantified UAC concentrations by measuring the height of the  $1510\text{ cm}^{-1}$   
222 aromatic (C=C) peak (Fig. 1), because this peak records changes in the abundance of the  
223 phenolic compounds *para*-coumaric acid and ferulic acid that act as UACs in sporopollenin  
224 (Fraser et al., 2014; Watson et al., 2007). Absorbance values in IR spectra relate to the  
225 thickness of material being analysed, so following previous research (Fraser et al., 2011;  
226 Jardine et al., 2015, 2016, 2017; Lomax et al., 2008, 2012) the  $1510\text{ cm}^{-1}$  aromatic peak  
227 height was normalized against the hydroxyl (OH) band centred on  $3300\text{ cm}^{-1}$  (Figure 1).  
228 Although the aromatic/OH ratio has not yet been calibrated to UAC concentrations or UV  
229 levels, it does provide a successful proxy whereby higher aromatic/OH ratio values equate to  
230 higher UV-B flux (Fraser et al., 2011; Jardine et al., 2016, 2017; Lomax et al., 2008, 2012).  
231 Short-term variations in ambient UV-B flux experienced by the pollen-producing plants will  
232 add noise to the UAC reconstruction; possible sources of additional variability are considered

233 in the Discussion. The raw data (sample ages and peak height measurements) are available for  
234 download from figshare (Jardine et al., 2019). [NB For review please used this private link  
235 to access the data: <https://figshare.com/s/45c1f29f1d76c1cbc01d>].

236

237 **[Insert Figure 1]**

238

239 We used the historical SSI reconstruction of Lean (2018) to obtain solar UV-B  
240 irradiance estimates for the last 650 years. This SSI reconstruction covers the period 850 to  
241 2016, and provides an annually resolved time series that incorporates information from space-  
242 based irradiance observations, sunspots and cosmogenic radionuclides (full details in Lean  
243 2018). Within the ultraviolet the SSI estimates are resolved to 1 nm wavebands. We therefore  
244 integrated the irradiance values within the range 280 to 315 nm, to obtain an irradiance  
245 reconstruction integrated across the UV-B part of the solar spectrum (shown in Figure 2b).

246

247 We used Spearman's rank order correlation to test the association between UACs and  
248 solar UV-B. For the UACs we used the mean of the five replicates within each pollen sample,  
249 and for solar UV-B we used the mean UV-B irradiance values within the calendar years  
250 represented by each pollen sample. Spearman's rank order correlation is appropriate because  
251 it is a non-parametric test that does not assume normality of distributions or a linear  
252 relationship among variables. To examine the influence of shared long-term temporal trends  
253 among the variables, we detrended the data by taking the residuals from linear regressions of  
254 each variable against time. The residuals were then used as variables in the correlation test.

255

## 256 **Results**

257 The Nar Gölü *Pinus* UAC record (Figure 2a) shows that surface level UV-B irradiance  
258 has varied over the last 650 years. Visual comparison with the solar UV-B reconstruction of

259 Lean (2018) (Figure 2b) reveals many of the same features, including an initial high value at  
260 ~ 1350, minima at ~1460 to 1550 (the Spörer Minimum), 1645 to 1710 (the Maunder  
261 Minimum), ~1790 to 1820 (the Dalton Minimum), and 1880 to 1920, and the rise from the  
262 Maunder Minimum to the late 20<sup>th</sup> Century. The Spearman's rank order correlation between  
263 the UAC data and solar UV-B reconstruction demonstrates statistically significant positive  
264 relationships for both raw ( $n = 28$ ,  $r_s = 0.52$ ,  $p = 0.005$ ) and detrended datasets ( $n = 28$ ,  $r_s =$   
265  $0.55$ ,  $p = 0.004$ ) (Figure 3). These correlations show that the visual similarities between the  
266 surface and solar UV-B data are robust.

267

268 **[Insert Figure 2]**

269

270 **[Insert Figure 3]**

271

## 272 **Discussion**

273 Our results show a positive correlation between the *Pinus* UAC data and the solar UV-  
274 B reconstruction of Lean (2018), demonstrating that solar activity and surface UV-B trends  
275 have been concordant over the last 650 years. These results are in agreement with the  
276 cladoceran-based surface UV-B reconstructions of Nevalainen et al. (2015, 2016, 2018), but  
277 are not consistent with the hypothesis of Rozema et al. (2002) that surface level UV-B should  
278 be anti-correlated with solar activity across grand solar minima and maxima. Our results  
279 therefore suggest that any variations in the thickness of the ozone layer were not sufficient to  
280 alter the incoming UV-B flux.

281

282 These results also demonstrate that the anti-correlation between solar activity and  
283 ground-based measurements of UV across the 11 year solar cycle (Rampelotto et al., 2009)  
284 cannot simply be scaled up to longer timescales (Rozema et al., 2002). Whether this implies a

285 different relationship between solar activity, UV and ozone thickness across the 11 year solar  
286 cycle and longer-term cycles and trends is currently unclear. While solar UV irradiance at  
287 wavelengths under 242 nm leads to ozone production, longer wavelength UV destroys it (Ball  
288 et al., 2016), therefore given the right balance of change across the UV spectrum decreases in  
289 ozone creation across solar minima could be cancelled out by decreases in ozone destruction  
290 (and vice versa during solar maxima). Ozone concentrations are also modulated by hydrogen,  
291 nitrogen, and chlorine catalytic cycles (Lary, 1997), and long-term variations in the  
292 atmospheric concentrations of HO<sub>x</sub>, NO<sub>x</sub> and ClO<sub>x</sub> radicals may influence how ozone  
293 thickness changes in response to solar UV. This question deserves further research, both with  
294 more instrumental measurements of spectral UV irradiance and surface level UV-B, and  
295 additional high-resolution UAC-based records over longer timescales.

296

297 While the relationships between our UAC data and solar UV-B are statistically  
298 significant (Figure 3), the strength of the correlations are moderate ( $r_s = 0.52$  for the raw data,  
299 and  $r_s = 0.55$  for the detrended data). In the Nar Gölü record we have identified three main  
300 factors that, in addition to solar UV-B, may have been responsible for variation in the UAC  
301 signal. First, the *Pinus* pollen does not represent local vegetation, but is thought to be largely  
302 sourced from the Taurus Mountains (England et al., 2008). The pollen signal therefore likely  
303 represents a mix of altitudes and incoming UV-B levels (Lomax et al., 2012), which will  
304 contribute to within-sample variance (Seddon et al., 2019). To the extent that the UV-B  
305 response differs among the *Pinus* species contributing pollen to the Nar Gölü record, any  
306 variations in their relative abundances over time may have added further noise to the UAC  
307 signal. The recently planted *Pinus* trees near Nar Gölü (England et al., 2008) may also have  
308 impacted upon the UAC measurement from the most recent sample in the record, which  
309 covers the years 1998 to 2001.

310

311 Second, variations in cloud cover modify surface UV irradiance levels (Calbó et al.,  
312 2005; Fraser et al., 2011). Although the UAC proxy is unlikely to be affected by short-term  
313 variations in cloudiness (Lomax et al., 2012), interannual variability in cloud cover may add  
314 additional noise to UAC time series where each sample represents several years of pollen  
315 release.

316

317 Third, any errors in the sediment core chronology will add noise to the correlations.  
318 Although dating precision in the Nar Gölü record is thought to be better than the maximum  
319 age uncertainty of 2.5% would suggest (Dean et al., 2013), small errors are likely to be  
320 inevitable even in continuously varved sediments, and the magnitude of change in solar UV-B  
321 irradiance across the 11 year solar cycle (Figure 2b; Lean, 2018) suggests that age model  
322 deviations could add substantial noise to the UAC-UV relationship. While dating errors of a  
323 few years could artificially impose a positive correlation between the solar UV-B  
324 reconstruction and UAC data, the sustained, multi-decadal solar UV-B lows during both the  
325 Spörer Minimum and Maunder Minimum (Figure 2b) coincide with intervals of low UAC  
326 concentrations (Figure 2a). This suggests that the positive correlation demonstrated here is not  
327 an artefact of minor errors in the varve chronology, but rather represents a genuine signal.

328

329 Despite these sources of variability, the UAC proxy has successfully recovered the  
330 major solar UV-B signal, demonstrating that it has much to offer as a means of examining  
331 solar inputs to the Earth system and their contributions to biotic and climatic change. As a  
332 surface UV-B proxy UAC measurements allow us to test hypotheses relating to changes in  
333 ozone thickness through time (Lomax et al., 2008), and can aid in deconvoluting the effects of  
334 solar activity and ozone-related variations on UV-B at the Earth's surface. The pollen UAC  
335 proxy could also be used in conjunction with UV proxies based on aquatic organisms  
336 (Nevalainen et al., 2016) to separate out solar UV from water transparency effects

337 (Nevalainen et al., 2015, 2018), and therefore constrain key factors impacting on aquatic  
338 ecosystems. More generally, the UAC proxy can be used to test for the impacts of surface  
339 UV-B changes on biotic systems, in relation to solar UV irradiance variations, longer term  
340 cycles in the Earth's orbit around the Sun (Jardine et al., 2016), and periods of ozone layer  
341 disruption (Lomax et al., 2008; Visscher et al., 2004).

342

343 Our *Pinus* UAC data, taken together with the cladocera data of Nevalainen et al.  
344 (2015, 2016, 2018), demonstrate that variations in solar UV irradiance are sufficient to drive  
345 biochemical responses in disparate environments and groups of organisms. Future changes in  
346 surface UV-B flux, whether driven by variations in solar activity or atmospheric composition,  
347 will alter not just organismal stress but also the metabolic costs of producing UV protective  
348 compounds, and may influence interspecific competitive relationships and ecosystem-level  
349 processes such as decomposition and carbon cycling (Rozema et al., 1997). The relative  
350 importance of these responses therefore needs to be assessed in future studies of ecological  
351 change.

352

### 353 **Conclusions**

354 We have provided the first detailed proxy reconstruction of surface level UV-B flux  
355 on centennial timescales. By linking this with a published solar UV-B reconstruction, we have  
356 shown that solar UV-B flux at the surface follows a similar long-term trend to top of  
357 atmosphere UV-B. On the timescales considered here, incoming solar UV flux will therefore  
358 be the dominant control on surface-level UV, rather than UV modulated ozone thickness. In  
359 addition to better understanding and modelling sources of variance in UAC reconstructions,  
360 future research in this area needs to focus on calibrating the UAC UV-B proxy to a specific  
361 dose-response relationship, to quantify the magnitude of change across different timescales  
362 (Rozema et al., 2001, 2002, 2009; Seddon et al., 2019). Developing an action spectrum

363 (Herman, 2010; Rozema et al., 2001; Seddon et al., 2019) for UAC production will also be  
364 important for quantifying how UAC concentrations vary with changes in ozone levels.  
365 Together, these measures will help towards understanding how variations in solar UV  
366 irradiance impact on Earth's climate and biota through time, both in the past and in the future.

367

### 368 **Acknowledgements**

369 The raw data for this study are available on figshare:

370 <https://dx.doi.org/10.6084/m9.figshare.8075519> [NB For review please used this private

371 link to access the data: <https://figshare.com/s/45c1f29f1d76c1cbc01d>]. We thank NERC

372 (grant NE/K005294/1) for funding this research, and a previous NERC award

373 (NER/S/A/2002/10316) to University of Birmingham-based PhD student, Ann England. Andy

374 Moss is thanked for lab support. We also thank Benjamin Bell and Liisa Nevalainen for

375 insightful reviews, and the anonymous reviewers whose comments improved earlier versions

376 of this paper.

377

### 378 **References**

379 Ball WT, Haigh JD, Rozanov EV, et al. (2016) High solar cycle spectral variations

380 inconsistent with stratospheric ozone observations. *Nature Geoscience* 9: 206-209.

381 Bell, BA. (2018) *Advancing the Application of Analytical Techniques in the Biological*

382 *Chemistry of Sporopollenin: Towards Novel Plant Physiological Tracers in*

383 *Quaternary Palynology*. PhD Thesis, University of Manchester, UK.

384 Bell BA, Fletcher WJ, Ryan P, et al. (2018) UV-B-absorbing compounds in modern *Cedrus*

385 *atlantica* pollen: The potential for a summer UV-B proxy for Northwest Africa. *The*

386 *Holocene* 28: 1382-1394.

387 Blokker, P, Boelen, P, Broekman, R and Rozema, J. (2006) The occurrence of *p*-coumaric  
388 acid and ferulic acid in fossil plant materials and their use as UV-proxy. *Plant Ecology*  
389 182: 197-207.

390 Blokker, P, Yeloff, D, Boelen, P, Broekman, R and Rozema, J. (2005). Development of a  
391 proxy for past surface UV-B irradiation: A thermally assisted hydrolysis and  
392 methylation py-GC/MS method for the analysis of pollen and spores. *Analytical*  
393 *Chemistry* 77: 6026-6031.

394 Calbó J, Pagès D and González J-A. (2005) Empirical studies of cloud effects on UV  
395 radiation: A review. *Reviews of Geophysics* 43.

396 Caldwell MM, Björn LO, Bornman JF, et al. (1998) Effects of increased solar ultraviolet  
397 radiation on terrestrial ecosystems. *Journal of Photochemistry and Photobiology B:*  
398 *Biology* 46: 40-52.

399 Christie JM, Arvai AS, Baxter KJ, et al. (2012) Plant UVR8 photoreceptor senses UV-B by  
400 tryptophan-mediated disruption of cross-dimer salt bridges. *Science* 335: 1492-1496.

401 Dean JR, Jones MD, Leng MJ, et al. (2015) Eastern Mediterranean hydroclimate over the late  
402 glacial and Holocene, reconstructed from the sediments of Nar lake, central Turkey,  
403 using stable isotopes and carbonate mineralogy. *Quaternary Science Reviews* 124:  
404 162-174.

405 Dean JR, Jones MD, Leng MJ, et al. (2013) Palaeo-seasonality of the last two millennia  
406 reconstructed from the oxygen isotope composition of carbonates and diatom silica  
407 from Nar Gölü, central Turkey. *Quaternary Science Reviews* 66: 35-44.

408 England A, Eastwood WJ, Roberts CN, et al. (2008) Historical landscape change in  
409 Cappadocia (central Turkey): a palaeoecological investigation of annually laminated  
410 sediments from Nar lake. *The Holocene* 18: 1229-1245.



411 Ermolli I, Matthes K, Dudok de Wit T, et al. (2013) Recent variability of the solar spectral  
412 irradiance and its impact on climate modelling. *Atmospheric Chemistry and Physics*  
413 13: 3945-3977.

414 Fraser WT, Lomax BH, Jardine PE, et al. (2014) Pollen and spores as a passive monitor of  
415 ultraviolet radiation. *Frontiers in Ecology and Evolution* 2.

416 Fraser WT, Scott AC, Forbes AES, et al. (2012) Evolutionary stasis of sporopollenin  
417 biochemistry revealed by unaltered Pennsylvanian spores. *New Phytologist* 196: 397-  
418 401.

419 Fraser WT, Sephton MA, Watson JS, et al. (2011) UV-B absorbing pigments in spores:  
420 biochemical responses to shade in a high-latitude birch forest and implications for  
421 sporopollenin-based proxies of past environmental change. *Polar Research* 30: 8312.

422 Gao W, Zheng Y, Slusser JR, et al. (2004) Effects of Supplementary Ultraviolet-B Irradiance  
423 on Maize Yield and Qualities: A Field Experiment. *Photochemistry and Photobiology*  
424 80: 127-131.

425 Gehrke C, Johanson U, Callaghan TV, et al. (1995) The impact of enhanced ultraviolet-B  
426 radiation on litter quality and decomposition processes in *Vaccinium* leaves from the  
427 Subarctic. *Oikos* 72: 213-222.

428 Gray LJ, Beer J, Geller M, et al. (2010) Solar Influences on Climate. *Reviews of Geophysics*  
429 48.

430 Haberreiter M, Schöll M, Dudok de Wit T, et al. (2017) A new observational solar irradiance  
431 composite. *Journal of Geophysical Research: Space Physics* 122: 5910-5930.

432 Herman JR. (2010) Use of an improved radiation amplification factor to estimate the effect of  
433 total ozone changes on action spectrum weighted irradiances and an instrument  
434 response function. *Journal of Geophysical Research* 115.

435 Ineson S, Maycock AC, Gray LJ, et al. (2015) Regional climate impacts of a possible future  
436 grand solar minimum. *Nature Communications* 6: 7535.

437 Jardine PE, Abernethy FAJ, Lomax BH, et al. (2017) Shedding light on sporopollenin  
438 chemistry, with reference to UV reconstructions. *Review of Palaeobotany and*  
439 *Palynology* 238: 1-6.

440 Jardine PE, Fraser, WT, Gosling, WD, et al. (2019) Data from “Reconstruction of ultraviolet-  
441 B irradiance at the Earth’s surface, and its relationship with solar activity and ozone  
442 thickness”. figshare, <https://dx.doi.org/10.6084/m9.figshare.8075519>.

443 Jardine PE, Fraser WT, Lomax BH, et al. (2015) The impact of oxidation on spore and pollen  
444 chemistry. *Journal of Micropalaeontology* 34: 139-149.

445 Jardine PE, Fraser WT, Lomax BH, et al. (2016) Pollen and spores as biological recorders of  
446 past ultraviolet irradiance. *Scientific Reports* 6: 1-8.

447 Jones MD, Leng MJ, Roberts CN, et al. (2005) A Coupled Calibration and Modelling  
448 Approach to the Understanding of Dry-Land Lake Oxygen Isotope Records. *Journal*  
449 *of Paleolimnology* 34: 391-411.

450 Jones MD, Roberts CN, Leng MJ, et al. (2006) A high-resolution late Holocene lake isotope  
451 record from Turkey and links to North Atlantic and monsoon climate. *Geology* 34:  
452 361.

453 Krivova NA, Vieira LEA and Solanki SK. (2010) Reconstruction of solar spectral irradiance  
454 since the Maunder minimum. *Journal of Geophysical Research* 115.

455 Lary DJ. (1997) Catalytic destruction of stratospheric ozone. *Journal of Geophysical*  
456 *Research: Atmospheres* 102: 21515-21526.

457 Lean JL. (2018) Estimating Solar Irradiance Since 850 CE. *Earth and Space Science* 5: 133-  
458 149.

459 Liland KH and Mevik B-H. (2015) baseline: Baseline Correction of Spectra. 1.2-1 ed.

460 Lomax BH, Fraser WT, Harrington G, et al. (2012) A novel palaeoaltimetry proxy based on  
461 spore and pollen wall chemistry. *Earth and Planetary Science Letters* 353-354: 22-28.

462 Lomax BH, Fraser WT, Sephton MA, et al. (2008) Plant spore walls as a record of long-term  
463 changes in ultraviolet-B radiation. *Nature Geoscience* 1: 592-596.

464 Mackenzie G, Boa AN, Diego-Taboada A, et al. (2015) Sporopollenin, The Least Known Yet  
465 Toughest Natural Biopolymer. *Frontiers in Materials* 2: 1-5.

466 Meijkamp B, Aerts R, van de Staaij J, et al. (1999) Effects of UV-B on secondary metabolites  
467 in plants. In: Rozema J (ed) *Stratospheric ozone depletion: The effects of enhanced*  
468 *UV-B on terrestrial ecosystems*. Leiden: Backhuys, 71-99.

469 Nevalainen L, Luoto TP, Rantala MV, et al. (2015) Role of terrestrial carbon in aquatic UV  
470 exposure and photoprotective pigmentation of meiofauna in subarctic lakes.  
471 *Freshwater Biology* 60: 2435-2444.

472 Nevalainen L, Rantala MV, Luoto TP, et al. (2016) Long-term changes in pigmentation of  
473 arctic *Daphnia* provide potential for reconstructing aquatic UV exposure. *Quaternary*  
474 *Science Reviews* 144: 44-50.

475 Nevalainen L, Rantala MV, Rautio M, et al. (2018) Spatio-temporal cladoceran  
476 (Branchiopoda) responses to climate change and solar radiation in subarctic ecotonal  
477 lakes. *Journal of Biogeography* 45: 1954-1965.

478 Rampelotto PH, da Rosa MB and Schuch NJ. (2009) Solar cycle and UV - B comparison for  
479 South America–South of Brazil (29° S, 53° W). In: Nakajima T and Yamasoe MA  
480 (eds) *AIP Conference Proceedings*. AIP, 490-493.

481 R Core Team (2017) R: A language and environment for statistical computing. 3.4.2 ed.  
482 Vienna, Austria: R Foundation for Statistical Computing.

483 Rizzini L, Favory JJ, Cloix C, et al. (2011) Perception of UV-B by the *Arabidopsis* UVR8  
484 Protein. *Science* 332: 103-106.

485 Rozema J, Blokker P, Mayoral Fuertes MA, et al. (2009) UV-B absorbing compounds in  
486 present-day and fossil pollen, spores, cuticles, seed coats and wood: evaluation of a

487 proxy for solar UV radiation. *Photochemical and Photobiological Sciences* 8: 1233-  
488 1243.

489 Rozema J, Broekman RA, Blokker P, et al. (2001) UV-B absorbance and UV-B absorbing  
490 compounds (*para*-coumaric acid) in pollen and sporopollenin: the perspective to track  
491 historic UV-B levels. *Journal of Photochemistry and Photobiology B: Biology* 62:  
492 108-117.

493 Rozema J, van de Staij J, Björn L-O, et al. (1997) UV-B as an environmental factor in plant  
494 life: stress and regulation. *Trends in Ecology and Evolution* 12: 22-28.

495 Rozema J, van Geel B, Björn L-O, et al. (2002) Toward Solving the UV Puzzle. *Science* 296:  
496 1621-1622.

497 Seddon AWR, Festi D, Robson TM, et al. (2019) Fossil pollen and spores as a tool for  
498 reconstructing ancient solar-ultraviolet irradiance received by plants: an assessment of  
499 prospects and challenges using proxy-system modelling. *Photochemical and*  
500 *Photobiological Sciences* 18: 275-294.

501 Singh SK, Reddy KR, Reddy VR, et al. (2014) Maize growth and developmental responses to  
502 temperature and ultraviolet-B radiation interaction. *Photosynthetica* 52: 262-271.

503 Solanki SK, Krivova NA and Haigh JD. (2013) Solar Irradiance Variability and Climate.  
504 *Annual Review of Astronomy and Astrophysics* 51: 311-351.

505 Steinhilber F, Abreu JA, Beer J, et al. (2012) 9,400 years of cosmic radiation and solar  
506 activity from ice cores and tree rings. *Proceedings of the National Academy of*  
507 *Sciences* 109: 5967-5971.

508 Svalgaard L and Schatten KH. (2016) Reconstruction of the Sunspot Group Number: The  
509 Backbone Method. *Solar Physics* 291: 2653-2684.

510 Usoskin IG. (2017) A history of solar activity over millennia. *Living Reviews in Solar Physics*  
511 14.

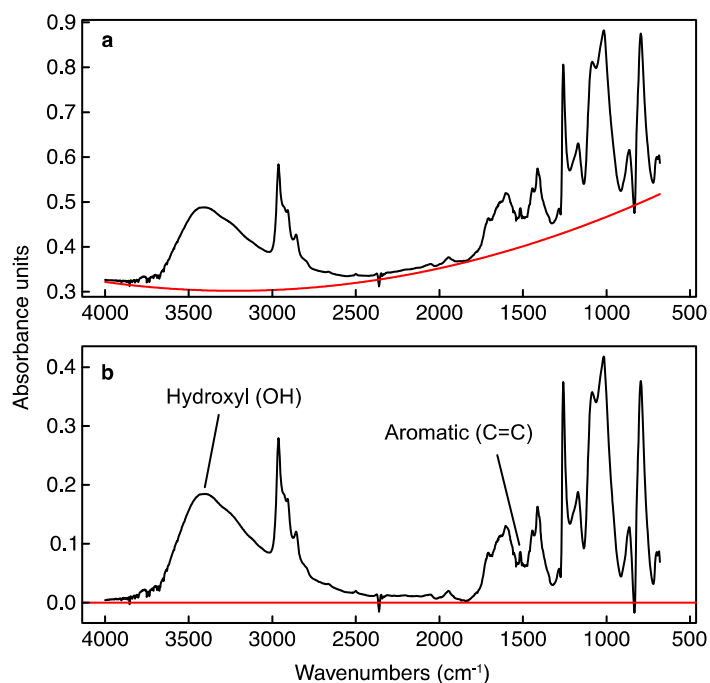
512 Visscher H, Looy CV, Collinson ME, et al. (2004) Environmental mutagenesis during the  
513 end-Permian ecological crisis. *Proceedings of the National Academy of Sciences of the*  
514 *United States of America* 101: 12952-12956.

515 Watson JS, Sephton MA, Sephton SV, et al. (2007) Rapid determination of spore chemistry  
516 using thermochemolysis gas chromatography-mass spectrometry and micro-Fourier  
517 transform infrared spectroscopy. *Photochemical and Photobiological Sciences* 6: 689-  
518 694.

519 Willis KJ, Feurdean A, Birks HJB, et al. (2011) Quantification of UV-B flux through time  
520 using UV-B-absorbing compounds contained in fossil *Pinus* sporopollenin. *New*  
521 *Phytologist* 192: 553-560.

522 Woldring, H and Bottema, S. (2003) The vegetation history of east-central Anatolia in  
523 relation to Archaeology: the Eski Acégöl pollen evidence compared with the Near  
524 Eastern environment. *Palaeohistoria* 43/44: 1-31.

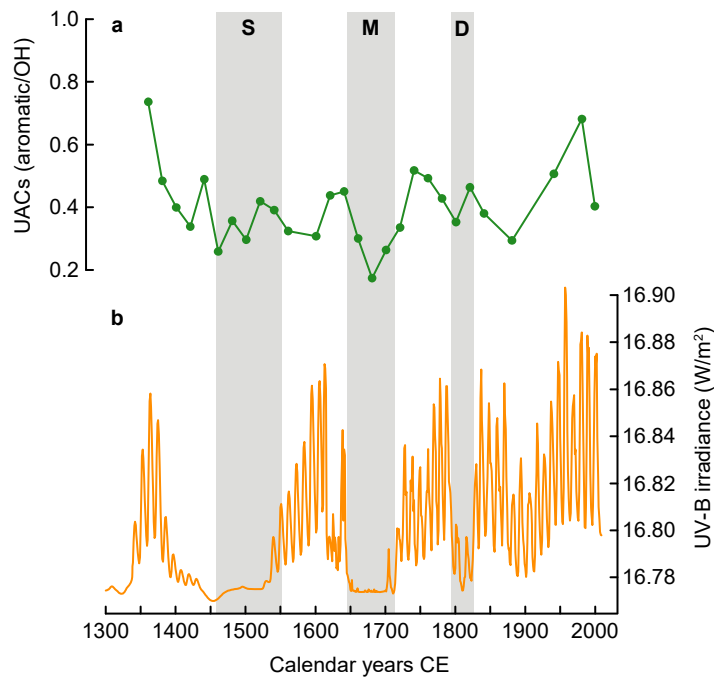
525



527

528 **Figure 1.** Representative chemical spectra of Nar Gölü *Pinus* pollen, from a sample dating  
529 from 1741 CE. (a) uncorrected spectrum showing fitted 2<sup>nd</sup> order polynomial baseline. (b)  
530 baseline corrected spectrum. The 1510 cm<sup>-1</sup> aromatic peak represents UV-B absorbing  
531 compounds (UACs) within pollen grains, and the 3300 cm<sup>-1</sup> hydroxyl band is used to  
532 normalize the peak height measurement.

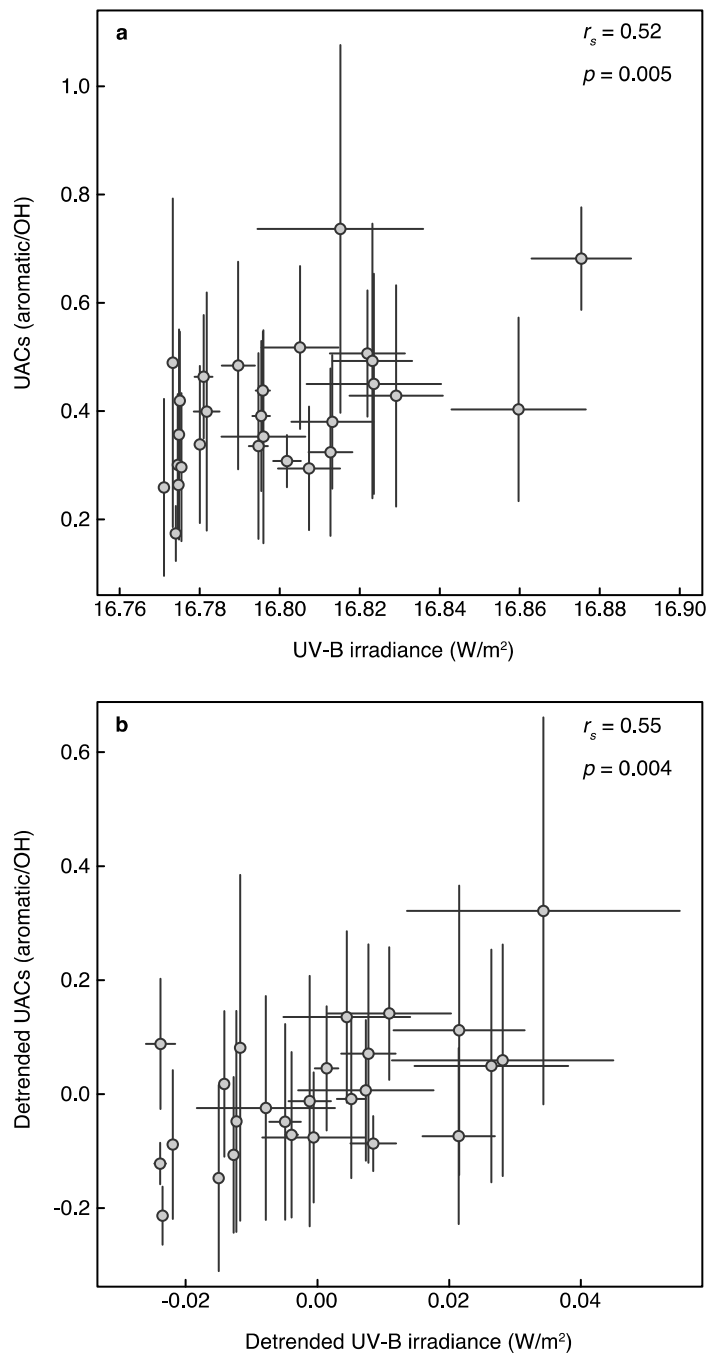
533



534

535 **Figure 2.** Surface and solar UV-B records. (a) Pinus UAC data from Nar Gölü, shown as the  
 536 mean of five replicates (solid green line with points showing samples)  $\pm 1$  standard deviation  
 537 (shaded area). (b) Modeled solar UV-B irradiance, from Lean (2018). Grey shaded regions  
 538 show solar minima, D = Dalton Minimum, M = Maunder Minimum, S = Spörer Minimum.

539



540

541 **Figure 3.** *Pinus* UAC data plotted against modeled solar UV-B irradiance (Lean 2018), for  
 542 both raw (a) and detrended (b) data. For the UAC data, the points show the mean of five  
 543 replicates, and the error bars are 1 standard deviation. For the UV-B irradiance reconstruction,  
 544 the points are the mean values within the calendar years represented by each pollen sample,  
 545 and the error bars are 1 standard deviation.  $r_s$  = Spearman's rank order correlation coefficient,  
 546  $p$  =  $p$  value of correlation.

547